Regional Embedding Enables High-Level Quantum Chemistry for Surface Science

Bryan T. G. Lau, 1 Gerald Knizia, 2, a) and Timothy C. Berkelbach 1, 3, b)

Compared to common density functionals, ab initio wave function methods can provide greater reliability and accuracy, which could prove useful when modeling adsorbates or defects of otherwise periodic systems. However, the breaking of translational symmetry necessitates large supercells that are often prohibitive for correlated wavefunction methods. As an alternative, this paper introduces the regional embedding approach, which enables correlated wavefunction treatments of *only* a target fragment of interest through small, fragment-localized orbital spaces constructed using a simple overlap criterion. Applications to the adsorption of water on lithium hydride, hexagonal boron nitride, and graphene substrates show that regional embedding combined with focal point corrections can provide converged CCSD(T) (coupled cluster) adsorption energies with very small fragment sizes.

In electronic structure theory, ab initio wave function methods provide a hierarchy of approximations that allow for systematic improvability-a feature missing in density functional theory (DFT). While ab initio methods were originally limited to molecules, advances in the past decade have enabled approaches like many-body perturbation theory or coupledcluster theory to be applied to atomistic periodic systems. 1-8 However, these methods are expensive and exploitation of translational symmetry is usually necessary to reduce their computational cost to manageable levels. Unfortunately, this is impossible in several applications scenarios of tremendous practical importance. For example, in models of crystal defects (e.g. for doping in semiconductor devices), or surface adsorbates (e.g. as involved in most core processes of heterogeneous catalysis), translational symmetry is broken. In practice, the non-periodic system is then described with supercells, which must be large in order to eliminate artifacts caused by the spurious interactions of the defect or adsorbate with its periodic images in other supercells. This is particularly problematic for ab initio methods, which are already expensive with translational symmetry.

However, when translational symmetry is broken by spatially-localized perturbations, the high cost of conventional treatments by large supercells is often artifical and can be avoided. To substantiate this claim, we here demonstrate that ab initio molecular adsorption energies can be obtained at significantly reduced cost, compared to the conventional supercell treatment, by a regional embedding technique. In general, the accurate prediction of noncovalent adsorption energies is challenging because they arise as small energy differences between large total energies. However, as opposed to total energies, adsorption energies are natural targets for regional embedding approaches, because they focus the computational effort on the important region of change. Like previous periodic embedding approaches, ^{10–13} we only correlate orbitals that are localized to a region near the adsorbate and can converge to the supercell result by increasing the size of the region. This

a) Electronic mail: knizia@psu.edu

technique allows us to perform expensive post-Hartree-Fock (HF) calculations on *only* the chemically important piece of the system, while retaining large supercells at the mean-field level to eliminate finite-size and finite-coverage effects. The new method adds to the large body of work on embedding and local correlation in periodic systems, including incremental 14–16 and hierarchical 17 expansions.

Unlike most previous embedding approaches, we localize the orbitals based upon their overlap with the fragment of interest in Hilbert space, rather than invoking real-space densities or localization functionals. The approach builds on quantum information concepts and, in particular, density matrix embedding theory (DMET). $^{18-20}$ DMET gives a precise prescription for the factorization of a system's wavefunction into active and inactive components, which we leverage to define a regional embedding procedure. For the orbitals occupied in the HF determinant of the entire system, we define an operator that projects onto a minimal atomic orbital (AO) basis of the atoms in the fragment A,

$$\hat{P}^{\text{occ}} = \sum_{\rho,\tau \in A}^{|a|} |\rho\rangle [\mathbf{S}^{-1}]_{\rho\tau} \langle \tau | \tag{1}$$

where ρ , τ are the minimal AO basis functions, S is the overlap matrix in the minimal AO basis, and |a| is the total number of minimal AO basis functions on the fragment. The eigenvectors of \hat{P}^{occ} in the basis of canonical occupied orbitals, $\mathbf{P}^{\text{occ}}\mathbf{V} = \mathbf{V} \operatorname{diag}\{\sigma_i\}$ with $P^{\text{occ}}_{ij} = \langle \varphi_i | \hat{P}^{\text{occ}} | \varphi_j \rangle$, define a rotated set of occupied orbitals whose eigenvalues $\{\sigma_i\}$ quantify their overlap with the fragment space. As a unitary transformation of the occupied orbitals, this procedure does not change the HF wavefunction, but merely separates the occupied orbitals into a set with nonzero overlap on the fragment (at most |a|) and a set with zero overlap on the fragment. If we were to use the same projection operator to rotate the canonical virtual orbitals, this procedure would generate the atomic valence active space²¹ of the fragment atoms. As explained by DMET, the combined active space would have at most 2|a| orbitals, which is the maximum number required to achieve a meanfield decoupling of the fragment minimal AOs from the rest of the system. However, this small active space lacks the basis

¹⁾Center for Computational Quantum Physics, Flatiron Institute, New York, New York 10010 USA

²⁾Department of Chemistry, Pennsylvania State University, University Park, Pennsylvania 16802 USA

³⁾Department of Chemistry, Columbia University, New York, New York 10027 USA

b) Electronic mail: tim.berkelbach@gmail.com

functions necessary for a description of dynamical correlation, which is critical for accurate adsorption energies. Therefore, we modify the procedure for the virtual space, defining the projection operator

$$\hat{P}^{\text{vir}} = \sum_{\mu,\nu \in A}^{|A|} |\mu\rangle [\mathbf{S}^{-1}]_{\mu\nu} \langle \nu| \tag{2}$$

where μ, ν are the *computational* AO basis functions used in the electronic structure calculation and |A| is the number of these basis functions on the fragment. Diagonalization in the basis of the canonical virtual orbitals, $\mathbf{P}^{\text{vir}}\bar{\mathbf{V}}=\bar{\mathbf{V}}\operatorname{diag}\{\sigma_a\}$ with $P_{ab}^{\text{vir}}=\langle\varphi_a|\hat{P}^{\text{vir}}|\varphi_b\rangle$, then defines a unitary transformation separating the virtuals into those with nonzero overlap on the fragment corresponding to eigenvalues $\sigma_a>0$ (at most |A|) and those with zero overlap on the fragment corresponding to eigenvalues $\sigma_a=0$. As discussed in Refs. 21 and 22, the combined occupied and virtual orbital spaces with fragment overlap are closely related to the combined impurity and bath orbital spaces in conventional DMET.

We propose to correlate only those orbitals that have significant overlap with the fragment, defined by a threshold on the eigenvalues σ of the projection operators. The rotated orbitals with insufficient overlap on the fragment space are simply frozen in the post-HF calculations, making the insertion of regional embedding into existing quantum chemistry workflows straightforward. Compared to other localization procedures, the one proposed here does not require minimization of a cost function (as in Foster-Boys, ²³ Edmiston-Ruedenberg, ²⁴ Pipek-Mezey, 25 or higher-order moment-based 26,27 localization) and does not result in nonorthogonal orbitals (as in projected atomic orbitals^{27–31}). We note that two recent works have explored similar overlap-based approaches to embedding, focusing on the occupied orbitals only³² and on multireference problems.³³ In future work we will compare the spatial extent and convergence properties of the local orbitals of these various approaches more thoroughly.

While any high-level quantum chemistry method may be used in the fragment calculation, here we focus on second-order Møller-Plesset perturbation theory (MP2) and coupled-cluster theory with single and double excitations (CCSD) and perturbative triples (CCSD(T)). These methods are valuable in this problem area for their nonempirical treatment of dispersion interactions. Furthermore, CCSD(T) is a powerful method in molecular thermochemistry: in small and electronically benign molecules, energy differences computed at its basis set limit typically deviate by ≤ 2 kJ/mol from the exact result, far outperforming all known DFT methods.³⁴ The extent to which this accuracy persists for the thermochemistry of solids and surfaces remains to be seen.

To test regional embedding, we study the adsorption of a water molecule on the (001) surface of lithium hydride (LiH), 35,36 hexagonal boron nitride (hBN), 6,37 and graphene. 15,38–40 These systems have been used to demonstrate the application of ab initio methods to periodic systems, and reference results obtained by extrapolation to the thermodynamic and complete basis set limits are available for a variety of DFT, wavefunction, and quantum Monte Carlo meth-

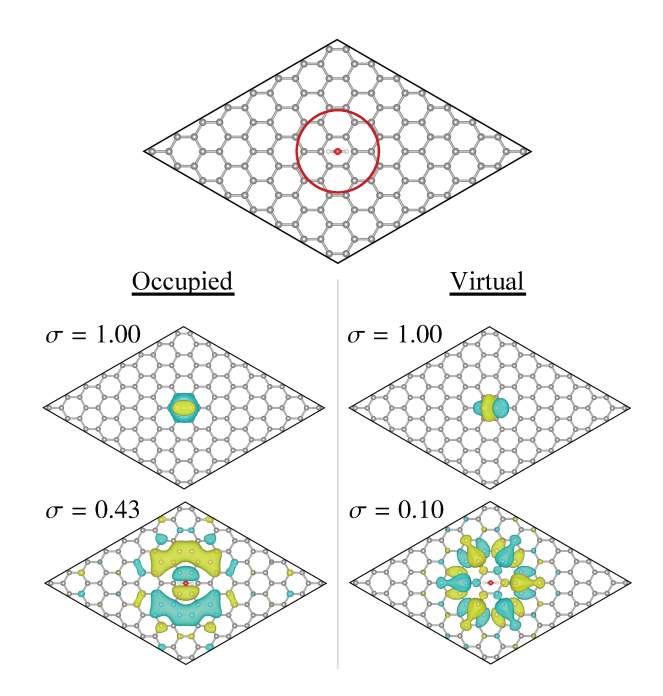


FIG. 1. An illustration of the embedding scheme used in this paper, for water on a 7×7 graphene supercell, with an example of randomly selected canonical and projected occupied orbitals. Carbon atoms from graphene are selected to be in the fragment based upon the radial distance from the oxygen atom in the water molecule.

ods.

We use literature values for the orientation and location of the water molecule on LiH³⁶ and hBN;³⁷ for water on graphene, we consider the so-called "0-leg" configuration.³⁹ The calculations are performed with slab geometries using a single layer of graphene and hBN and two layers of the LiH (001) plane along with 20 Å of vacuum in the direction perpendicular to the surface.

Figure 1 illustrates the method of selecting atoms in the fragment, using the example of water on graphene. The atoms of the water molecule are always included in the fragment and we add atoms from the substrate based upon their radial distance from the water molecule. In Figure 1 we also show the localized occupied and virtual orbitals with the most overlap (top row) and least nonzero overlap (bottom row) used in the subsequent post-HF calculations. The adsorption energy is found from three separate calculations,

$$E_{\text{ads}} = E_{\text{H}_2\text{O} + \text{substrate}} - E_{\text{H}_2\text{O}} - E_{\text{substrate}}.$$
 (3)

In order to apply the counterpoise correction for basis set superposition error,⁴¹ the HF calculations of the water and the substrate are performed in the full basis set of the combined system. In the post-HF step of each separate calculation, we apply the embedding procedure using the same eigenvalue cutoff in each.

All calculations are performed with periodic boundary conditions as implemented in PySCF, ^{42,43} using Gaussian density fitting ⁴⁴ of periodic integrals, GTH pseudopotentials, ⁴⁵ and their corresponding family of basis sets. We use the aug-

TZV2P basis set for the water molecule and a mixture of the DZVP and TZVP basis sets for the substrate. We use the SZV basis as the minimal AO basis required for projection of the occupied orbitals and the eigenvalue cutoff is set to $\sigma \geq 0.1$ for both the occupied and virtual space, although a number of other truncation procedures exist. We are in the process of exhaustively and systematically investigating optimal truncation procedures, which may depend on the system and properties of interest; we will publish these results elsewhere. Following truncation in the localized orbital basis, we rediagonalize the Fock matrix to obtain new canonical orbitals for the post-HF calculations. Generically, we observe that the numbers of occupied and virtual orbitals retained in the calculations grow proportional to the number of atoms included in the fragment. In the Supporting Information, we provide more details about the numerical performance of this embedding.

Figure 2 plots the MP2 adsorption energy as a function of the number of substrate atoms in the fragment for water on (a) LiH, (b) hBN, and (c) graphene for a series of supercell sizes, where we use the the DZVP basis for the substrate atoms. The reasonable cost of MP2 calculations allows us to increase the fragment size to the full supercell limit and thus carefully study the convergence. Interestingly, the convergence behaviors are quite different, reflecting the various electronic characters of the molecule-substrate interaction.

The adsorption energy of water on LiH, Figure 2a, smoothly converges to the full supercell limit, and the energy minimally changes as the supercell size is increased from 4×4 to 6×6 . These results reflect the highly local nature of the interaction of water with the highly insulating LiH (001) surface, which is captured at fragment sizes much smaller than the full supercell.

In contrast, the MP2 adsorption energy curves for hBN, Figure 2b, quickly reach a minimum before slowly rising to the full supercell energy. It is possible that the minimum value represents the most accurate energy for a given supercell size and that the rise in energy is due to error from the finite coverage of water. In other words, as the fragment grows in size, it includes orbitals that are erroneously perturbed by the periodic images, leading to a spurious interaction that raises the adsorption energy. However, as the supercell grows in size, the water molecule is further separated from its periodic images, and the fragment size can grow larger without including these unphysical orbitals. Another possibility is that the minimum occurs due to slightly different treatments of the separate calculations that contribute to the adsorption energy. In any event, the exact origin of this minimum is unclear and worthy of future study.

Finally, the MP2 adsorption energy of water on graphene, Figure 2c, exhibits a very slow convergence to the the supercell limit and shows no indication of absolute convergence. This behavior is almost surely due to the challenge of localizing orbitals in gapless materials^{27,46–48} and the closely related importance of long-range dispersion and polarization. As shown in Figure 1, the retained occupied and virtual orbitals with the smallest fragment overlaps have significant weight outside of the fragment. Moreover, the current embedding scheme does not allow the environment to respond

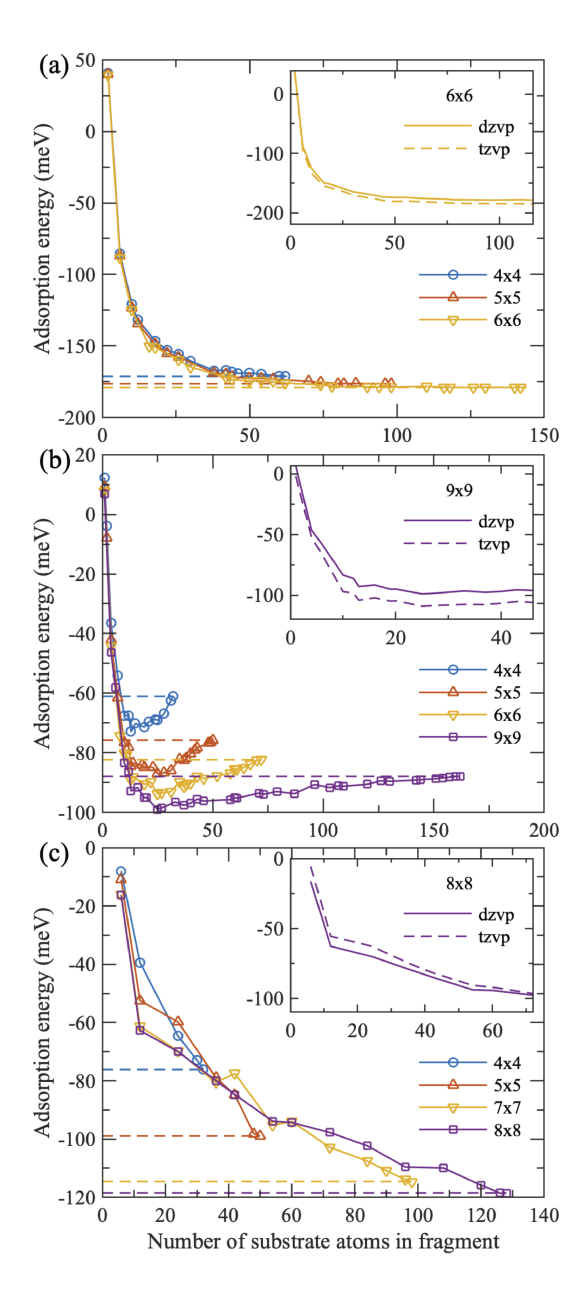


FIG. 2. The MP2 adsorption energy vs. fragment size, for water on (a) LiH, (b) hBN, and (c) graphene, with the DZVP basis on the substrate. The insets compare the DZVP and TZVP basis sets. The smaller DZVP basis allows for MP2 calculations of all fragment sizes up to the full supercell, the results of which are indicated by a dashed horizontal line.

to the correlated fragment; however, while a self-consistent embedding would in principle be desirable, we see no way of achieving it without sacrificing the simplicity of the presented regional embedding method.

The inset of each panel in Figure 2 shows a comparison to results obtained by using the TZVP basis for the substrate atoms in the fragment (and DZVP for the substrate atoms outside of the fragment). These latter calculations are limited in size by memory or convergence issues associated with linear dependencies in periodic systems. Using the larger TZVP

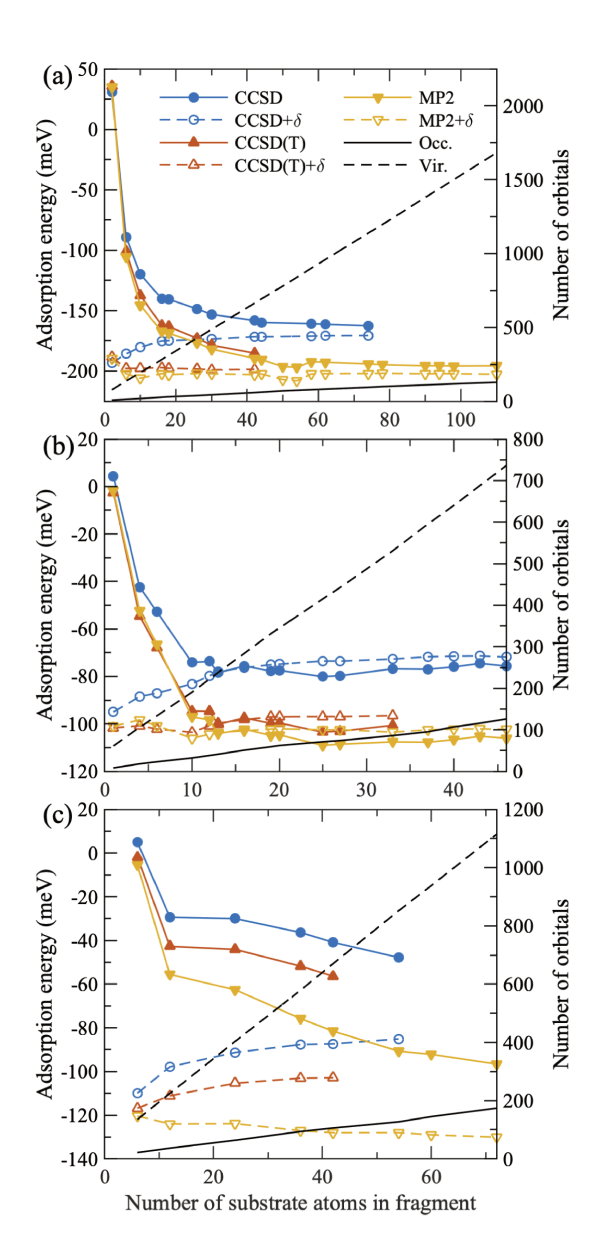


FIG. 3. The post-HF adsorption energy as a function of fragment size, for water on (a) 6×6 LiH, (b) 9×9 hBN, and (c) 8×8 graphene, with TZVP on the substrate fragment atoms and DZVP on the rest of the substrate. The solid lines with filled symbols correspond to uncorrected values, while the dashed lines with open symbols correspond to finite-size (FS) corrected values, as described in the text. The solid and dashed lines plot the number of occupied and virtual orbitals that are correlated in the post-HF calculation (right y-axis).

basis on the fragment does not qualitatively alter the convergence behavior and changes the adsorption energy by 10 meV or less.

In Figure 3, we present our main results of the adsorption energy obtained using MP2, CCSD, and CCSD(T), for the same three systems with the largest supercell sizes considered, i.e. 6×6 for LiH, 9×9 for hBN, and 8×8 for graphene. As in the insets of Figure 2, all calculations use the TZVP basis for the substrate atoms belonging to the fragment and DZVP for the remainder, except for the (T) correction, which used the

	LiH		hBN		graphene	
	present	lit. ³⁶	present	lit.	present	lit. ³⁹
MP2	192	233	102	110, ³⁷ 118 ⁶	130	-
CCSD	171	229	72	84^{6}	85	-
CCSD(T)	199	254	97	103^{6}	103	87

TABLE I. Adsorption energy of a water molecule on LiH, hBN, and graphene, comparing results obtained in the present manuscript and in the literature (lit.). All energies are in meV.

DZVP basis for all substrate atoms,

$$E_{\text{CCSD(T)}}(N, \text{TZ}) = E_{\text{CCSD}}(N, \text{TZ}) + \delta^{(\text{T})}(N, \text{DZ}),$$

$$\delta^{(\text{T})} = [E_{\text{CCSD(T)}} - E_{\text{CCSD}}](N, \text{DZ}),$$
(4)

where N is the number of fragment atoms and E is the adsorption energy. The adsorption energies, plotted with solid lines and filled symbols, follow the same shape and rate of convergence as the MP2 results presented in Figure 2. In particular, the shape of convergence correlates with the adsorption energy, as seen when comparing the strong, local adsorption of water on LiH versus the dispersion-dominated interaction with hBN and graphene.

Given the similar convergence behavior of the adsorption energies and the relatively cheap cost of MP2, we can correct the results by using a simple composite (focal-point) scheme,

$$E(\infty, TZ) = E(N, TZ) + \delta(N, DZ)$$

$$\delta(N, DZ) = [E_{MP2}(\infty) - E_{MP2}(N)] (DZ),$$
 (5)

where we estimate $E_{\rm MP2}(\infty)$, the MP2 adsorption energy in the thermodynamic limit, by a 1/N extrapolation of a series of full supercell MP2 calculations (further discussion of this extrapolation is provided in the Supporting Information). The above correction can be understood physically in a variety of ways, e.g. as a finite-size correction to the fragment result, as a fragment-level correction to the extrapolated MP2/DZVP result, or as an approximation to the missing dynamical correlation of frozen orbitals. When we apply this correction, we find that our data are frequently converged to within 10 meV when correlating only five to ten atoms in the substrate!

Considering differences in implementation details, our results compare favorably to recent literature values, ^{6,36,37,39} as shown in Table I. Our preliminary testing indicates that the primary source of discrepancy is basis set error due to our use of GTH basis sets. In the Supporting Information, we show MP2 results for water on LiH using correlation consistent effective core potentials and their associated basis sets⁴⁹ and we find that the discrepancy with literature values is halved, from about 40 meV to about 20 meV. We emphasize that previous calculations for all three systems have only been performed on 4×4 supercells and then extrapolated to correct for finitesize effects. In contrast, our approach allows us to directly simulate much larger supercells up to 9×9 , and monitor the convergence as a function of the number of atoms in the local fragment. Taken together, the combination of regional embedding and focal point corrections (for basis set and finite-size

effects) enables the calculation of high-quality ab initio adsorption energies at very low computational cost.

In summary, we have presented regional embedding, which allows an isolated treatment of local chemical changes with high level wave function methods. This is achieved by unitary transformations of the occupied and virtual Hartree-Fock orbitals based on the degree of overlap with the fragment's Hilbert space. The conventional use of high level wave functions in sufficiently large supercells is expensive. In contrast, regional embedding restricts the correlated calculation to the Hilbert space associated with the target fragment; consequently, large supercells can be used and the finite-size error can be efficiently eliminated. The benchmarks presented indicate that regional embedding with finite-size (focal point) corrections allows remarkably quick convergence to the thermodynamic limit, although the rate of convergence depends on the nature of molecule-substrate interaction. Converged results are achieved with correlated calculations on much smaller systems than the supercells used in contemporary periodic quantum chemistry and quantum Monte Carlo methods.

We expect this method to have broad applicability in molecular, biological, and condensed systems. The simplicity and performance should make it an appealing choice whenever modeling localized chemical changes in large systems. This covers many application scenarios, and we have already started projects in heterogeneous catalysis and in the optical and thermochemical properties of crystal defects. Concerning the theory, treating the frozen orbitals at levels beyond focal-point corrections may further increase the power of the method; self-consistent quantum embeddings, canonical transformations, or screened interactions may provide viable avenues. Finally, a core appeal of this method is that the embedded quantum system can be handled with essentially arbitrary many-body solvers, including quantum chemical multireference methods for strongly correlated systems. This may open a pathway to reliable treatments of complex electronic structure phenomena also in condensed phases and at interfaces. For example, these methods can be used to address long-standing problems in catalyst doping, catalysis at surface defects (e.g. kinks and edges), or the surface chemistry of transition metals and radicals.

ASSOCIATED CONTENT

Supporting Information

The Supporting Information is available free of charge at [xxx]. Numerical results for the eigenvalues of the projection operators and the retained orbital numbers, finite-size extrapolation of MP2 adsorption energies, and MP2 results for water on LiH with an alternative pseudopotential and correlation-consistent basis set.

ACKNOWLEDGMENTS

T.C.B. thanks Sandeep Sharma for helpful discussions. This work was supported in part by the NSF CAREER program under award No. CHE-1945276 (G.K.) and by the NSF Cyberinfrastructure for Sustained Scientific Innovation program via award No. OAC-1931321 (T.C.B.). The Flatiron Institute is a division of the Simons Foundation.

REFERENCES

- ¹Marsman, M.; Grüneis, A.; Paier, J.; Kresse, G. Second-Order Møller–Plesset Perturbation Theory Applied to Extended Systems. I. Within the Projector-Augmented-Wave Formalism Using a Plane Wave Basis Set. *J. Chem. Phys.* **2009**, *130*, 184103.
- ²Müller, C.; Paulus, B. Wavefunction-based electron correlation methods for solids. *Phys. Chem. Chem. Phys.* **2012**, *14*, 7605–7614.
- ³Booth, G. H.; Grüneis, A.; Kresse, G.; Alavi, A. Towards an Exact Description of Electronic Wavefunctions in Real Solids. *Nature* **2013**, *493*, 365–370.
- ⁴Yang, J.; Hu, W.; Usvyat, D.; Matthews, D.; Schütz, M.; Chan, G. K.-L. Ab Initio Determination of the Crystalline Benzene Lattice Energy to Sub-Kilojoule/Mole Accuracy. *Science* **2014**, *345*, 640–643.
- ⁵McClain, J.; Sun, Q.; Chan, G. K.-L.; Berkelbach, T. C. Gaussian-Based Coupled-Cluster Theory for the Ground-State and Band Structure of Solids. *J. Chem. Theory Comput.* **2017**, *13*, 1209–1218.
- ⁶Gruber, T.; Liao, K.; Tsatsoulis, T.; Hummel, F.; Grüneis, A. Applying the Coupled-Cluster Ansatz to Solids and Surfaces in the Thermodynamic Limit. *Phys. Rev. X* **2018**, *8*, 021043.
- ⁷Zhang, I. Y.; Grüneis, A. Coupled cluster theory in materials science. *Front. Mater.* **2019**, *6*.
- ⁸Dovesi, R. et al. The CRYSTAL code, 1976–2020 and beyond, a long story. J. Chem. Phys. **2020**, 152, 204111.
- ⁹Maurer, R. J.; Ruiz, V. G.; Camarillo-Cisneros, J.; Liu, W.; Ferri, N.; Reuter, K.; Tkatchenko, A. Adsorption structures and energetics of molecules on metal surfaces: Bridging experiment and theory. *Prog. Surf. Sci.* 2016, 91, 72 100.
- ¹⁰Govind, N.; Wang, Y. A.; Carter, E. A. Electronic-Structure Calculations by First-Principles Density-Based Embedding of Explicitly Correlated Systems. *J. Chem. Phys.* **1999**, *110*, 7677–7688.
- ¹¹Chulhai, D. V.; Goodpaster, J. D. Projection-Based Correlated Wave Function in Density Functional Theory Embedding for Periodic Systems. *J. Chem. Theory Comput.* **2018**, *14*, 1928–1942.
- ¹² Virgus, Y.; Purwanto, W.; Krakauer, H.; Zhang, S. Stability, energetics, and magnetic states of cobalt adatoms on graphene. *Phys. Rev. Lett.* **2014**, *113*, 1–6.
- ¹³Eskridge, B.; Krakauer, H.; Zhang, S. Local Embedding and Effective Downfolding in the Auxiliary-Field Quantum Monte Carlo Method. *J. Chem. Theory Comput.* **2019**, *15*, 3949–3959.
- ¹⁴Stoll, H.; Paulus, B.; Fulde, P. On the accuracy of correlation-energy expansions in terms of local increments. *J. Chem. Phys.* 2005, 123, 144108.
- ¹⁵Voloshina, E.; Usvyat, D.; Schütz, M.; Dedkov, Y.; Paulus, B. On the physisorption of water on graphene: A CCSD(T) study. *Phys. Chem. Chem. Phys.* 2011, *13*, 12041–12047.
- ¹⁶Bygrave, P. J.; Allan, N. L.; Manby, F. R. The Embedded Many-Body Expansion for Energetics of Molecular Crystals. *J. Chem. Phys.* **2012**, *137*, 164102.
- ¹⁷Nolan, S. J.; Gillan, M. J.; Alfè, D.; Allan, N. L.; Manby, F. R. Calculation of properties of crystalline lithium hydride using correlated wave function theory. *Phys. Rev. B* **2009**, *80*, 165109.
- ¹⁸Knizia, G.; Chan, G. K.-L. Density Matrix Embedding: A Strong-Coupling Quantum Embedding Theory. *J. Chem. Theory Comput.* **2013**, *9*, 1428– 1432.
- ¹⁹Wouters, S.; Jiménez-Hoyos, C. A.; Sun, Q.; Chan, G. K. A Practical Guide to Density Matrix Embedding Theory in Quantum Chemistry. *J. Chem. Theory Comput.* **2016**, *12*, 2706–2719.

- ²⁰Cui, Z.-H.; Zhu, T.; Chan, G. K.-L. Efficient Implementation of Ab Initio Quantum Embedding in Periodic Systems: Density Matrix Embedding Theory. *J. Chem. Theory Comput.* **2020**, *16*, 119–129.
- ²¹ Sayfutyarova, E. R.; Sun, Q.; Chan, G. K.-L.; Knizia, G. Automated Construction of Molecular Active Spaces from Atomic Valence Orbitals. *J. Chem. Theory Comput.* **2017**, *13*, 4063–4078.
- ²²Zheng, B.-X.; Chan, G. K.-L. Ground-state phase diagram of the square lattice Hubbard model from density matrix embedding theory. *Phys. Rev. B* 2016, 93, 035126.
- ²³Foster, J. M.; Boys, S. F. Canonical Configurational Interaction Procedure. Rev. Mod. Phys. **1960**, 32, 300–302.
- ²⁴Edmiston, C.; Ruedenberg, K. Localized Atomic and Molecular Orbitals. Rev. Mod. Phys. 1963, 35, 457–464.
- ²⁵Pipek, J.; Mezey, P. G. A fast intrinsic localization procedure applicable for ab initio and semiempirical linear combination of atomic orbital wave functions. *J. Chem. Phys.* **1989**, *90*, 4916–4926.
- ²⁶Høyvik, I.-M.; Jansik, B.; Jørgensen, P. Orbital localization using fourth central moment minimization. J. Chem. Phys. 2012, 137, 224114.
- ²⁷Høyvik, I.-M.; Kristensen, K.; Kjærgaard, T.; Jørgensen, P. A perspective on the localizability of Hartree–Fock orbitals. *Theor. Chem. Acc.* **2014**, *133*, 1417.
- ²⁸Pulay, P. Localizability of dynamic electron correlation. *Chem. Phys. Lett* 1983, 100, 151 – 154.
- ²⁹Saebo, S.; Pulay, P. Local Treatment of Electron Correlation. Annu. Rev. Phys. Chem. 1993, 44, 213–236.
- ³⁰Hampel, C.; Werner, H. Local treatment of electron correlation in coupled cluster theory. J. Chem. Phys. 1996, 104, 6286–6297.
- ³¹Schütz, M.; Werner, H.-J. Low-order scaling local electron correlation methods. IV. Linear scaling local coupled-cluster (LCCSD). *J. Chem. Phys.* 2001, 114, 661–681.
- ³²Claudino, D.; Mayhall, N. J. Automatic Partition of Orbital Spaces Based on Singular Value Decomposition in the Context of Embedding Theories. *J. Chem. Theory Comput.* **2019**, *15*, 1053–1064.
- ³³He, N.; Evangelista, F. A. A zeroth-order active-space frozen-orbital embedding scheme for multireference calculations. *J. Chem. Phys.* **2020**, *152*, 094107.
- ³⁴Karton, A.; Rabinovich, E.; Martin, J. M.; Ruscic, B. W4 theory for computational thermochemistry: In pursuit of confident sub-kJ/mol predictions. *J. Chem. Phys.* **2006**, *125*, 144108.
- ³⁵Booth, G. H.; Tsatsoulis, T.; Chan, G. K.-L.; Grüneis, A. From plane waves to local Gaussians for the simulation of correlated periodic systems. *J. Chem. Phys.* **2016**, *145*, 084111.
- ³⁶Tsatsoulis, T.; Hummel, F.; Usvyat, D.; Schütz, M.; Booth, G. H.; Binnie, S. S.; Gillan, M. J.; Alfè, D.; Michaelides, A.; Grüneis, A. A compari-

- son between quantum chemistry and quantum Monte Carlo techniques for the adsorption of water on the (001) LiH surface. *J. Chem. Phys.* **2017**, *146*, 204108.
- ³⁷Al-Hamdani, Y. S.; Rossi, M.; Alfè, D.; Tsatsoulis, T.; Ramberger, B.; Brandenburg, J. G.; Zen, A.; Kresse, G.; Grüneis, A.; Tkatchenko, A.; Michaelides, A. Properties of the water to boron nitride interaction: From zero to two dimensions with benchmark accuracy. *J. Chem. Phys.* 2017, 147, 044710.
- ³⁸Jenness, G. R.; Karalti, O.; Jordan, K. D. Benchmark calculations of water–acene interaction energies: Extrapolation to the water–graphene limit and assessment of dispersion–corrected DFT methods. *Phys. Chem. Chem. Phys.* **2010**, *12*, 6375–6381.
- ³⁹Brandenburg, J. G.; Zen, A.; Fitzner, M.; Ramberger, B.; Kresse, G.; Tsatsoulis, T.; Grüneis, A.; Michaelides, A.; Alfè, D. Physisorption of Water on Graphene: Subchemical Accuracy from Many-Body Electronic Structure Methods. *J. Phys. Chem. Lett.* **2019**, *10*, 358–368.
- ⁴⁰Jordan, K. D.; Heßelmann, A. Comment on "Physisorption of Water on Graphene: Subchemical Accuracy from Many-Body Electronic Structure Methods". J. Phys. Chem. C 2019, 123, 10163–10165.
- ⁴¹Boys, S.; Bernardi, F. The calculation of small molecular interactions by the differences of separate total energies. Some procedures with reduced errors. *Mol. Phys.* **1970**, *19*, 553–566.
- ⁴²Sun, Q.; Berkelbach, T. C.; Blunt, N. S.; Booth, G. H.; Guo, S.; Li, Z.; Liu, J.; McClain, J. D.; Sayfutyarova, E. R.; Sharma, S.; Wouters, S.; Chan, G. K.-L. PySCF: the Python-based simulations of chemistry framework. Wires. Comput. Mol. Sci. 2018, 8, e1340.
- ⁴³Sun, Q. et al. Recent developments in the PySCF program package. J. Chem. Phys. 2020, 153, 024109.
- ⁴⁴Sun, Q.; Berkelbach, T. C.; McClain, J. D.; Chan, G. K.-L. Gaussian and plane-wave mixed density fitting for periodic systems. *J. Chem. Phys.* **2017**, 147, 164119.
- ⁴⁵Goedecker, S.; Teter, M.; Hutter, J. Separable dual-space Gaussian pseudopotentials. *Phys. Rev. B* **1996**, *54*, 1703–1710.
- ⁴⁶Maslen, P. E.; Ochsenfeld, C.; White, C. A.; Lee, M. S.; Head-Gordon, M. Locality and Sparsity of Ab Initio One-Particle Density Matrices and Localized Orbitals. *J. Phys. Chem. A* 1998, 102, 2215–2222.
- ⁴⁷Marzari, N.; Mostofi, A. A.; Yates, J. R.; Souza, I.; Vanderbilt, D. Maximally localized Wannier functions: Theory and applications. *Rev. Mod. Phys.* 2012, 84, 1419–1475.
- ⁴⁸Souza, I.; Marzari, N.; Vanderbilt, D. Maximally localized Wannier functions for entangled energy bands. *Phys. Rev. B* 2001, 65, 035109.
- ⁴⁹Wang, G.; Annaberdiyev, A.; Melton, C. A.; Bennett, M. C.; Shulenburger, L.; Mitas, L. A new generation of effective core potentials from correlated calculations: 4s and 4p main group elements and first row additions. *The Journal of Chemical Physics* 2019, 151, 144110.